

Simulation of quantum physics with Tensor Processing Units: brute-force computation of ground states and time evolution

Markus Hauru,¹ Alan Morningstar,^{2,1} Jackson Beall,¹ Martin Ganahl,¹ Adam Lewis,¹ and Guifre Vidal¹

¹*Sandbox@Alphabet, Mountain View, CA 94043, USA*

²*Department of Physics, Princeton University, Princeton, NJ 08544, USA*

(Dated: November 23, 2021)

Tensor Processing Units (TPUs) were developed by Google exclusively to support large-scale machine learning tasks. TPUs can, however, also be used to accelerate and scale up other computationally demanding tasks. In this paper we repurpose TPUs for the challenging problem of simulating quantum spin systems. Consider a lattice model made of N spin- $\frac{1}{2}$ quantum spins, or qubits, with a Hamiltonian $H = \sum_i h_i$ that is a sum of local terms h_i and a wavefunction $|\Psi\rangle$ consisting of 2^N complex amplitudes. We demonstrate the usage of TPUs for both (i) computing the ground state $|\Psi_{\text{gs}}\rangle$ of the Hamiltonian H , and (ii) simulating the time evolution $|\Psi(t)\rangle = e^{-itH} |\Psi(0)\rangle$ generated by this Hamiltonian starting from some initial state $|\Psi(0)\rangle$. The bottleneck of the above tasks is computing the product $H|\Psi\rangle$, which can be implemented with remarkable efficiency utilising the native capabilities of TPUs. With a TPU v3 pod, with 2048 cores, we simulate wavefunctions $|\Psi\rangle$ of up to $N = 38$ qubits. The dedicated matrix multiplication units (MXUs), the high bandwidth memory (HBM) on each core, and the fast inter-core interconnects (ICIs) together provide performance far beyond the capabilities of general purpose processors.

The study of quantum many-body phenomena in strongly correlated systems is among the most challenging computational tasks in modern physics. Describing the quantum mechanical wavefunction of a many-body system, say of N interacting quantum spins, requires computational resources that scale exponentially with the system size N . Sophisticated numerical approaches have been devised over the years to tackle such problems. For instance, Quantum Monte Carlo (QMC) methods bypass storing the full wavefunction by instead sampling over statistically significant configurations [1–3], whereas tensor network (TN) algorithms exploit the structure of entanglement in ground states of local Hamiltonians to obtain an efficient quasi-exact description [4–9]. These highly successful methods are customarily used to study emergent quantum phenomena at scale. They have, however, a restricted range of applicability. For instance, none of them can correctly simulate a long Hamiltonian evolution: QMC due to the sign problem, TNs due to the build-up of entanglement over time. In such situations, a brute-force computation requiring exponentially many resources is still today the only reliable approach. A brute-force computation, free of statistical and/or truncation errors, is also useful even in regimes where QMC and TN methods are expected to work, e.g. to benchmark their performance.

Google’s Tensor Processing Units (TPUs) are *application-specific integrated circuits* (ASICs) exclusively designed for accelerating training and inference of machine learning models at scale [10, 11]. Here we consider the third generation (v3) of TPUs. We can think of a TPU v3 *pod*, with 2048 cores, 100+ petaFLOPS (in half precision) and 32 TB of high bandwidth memory (HBM), as a special-purpose supercomputer. That is, instead of being designed for general purpose high performance computing (HPC) tasks, a TPU pod is a supercomputer optimized to excel at a class of specialized workloads required for machine learning. Neverthe-

less, one can still inquire whether TPUs’ acceleration and scalability may be repurposed for other computational tasks [12–26], in analogy with how Graphic Processing Units (GPUs), originally conceived to accelerate the rendering of 3D graphics in gaming, have extended to a much broader range of applications, including general purpose HPC and artificial intelligence.

In this paper we explain how to use TPUs for brute-force simulations of quantum many-body physics. In short, the wavefunction $|\Psi\rangle$ of N spin- $\frac{1}{2}$ quantum spins, or qubits, is distributed over the available HBM and then updated under the action of a local Hamiltonian H ,

$$|\Psi\rangle \mapsto |\Psi'\rangle = H|\Psi\rangle, \quad (1)$$

which requires both large matrix multiplications on each TPU core and repeatedly re-distributing the wavefunction over the cores. Matrix multiplications and wavefunction re-distribution are handled by the TPU’s remarkably fast *matrix multiply units* (MXUs) and inter-core interconnects (ICIs), respectively. Fig. 1 shows typical update times for up to $N = 38$ qubits.

The ability to update the wavefunction $|\Psi\rangle$ according to Eq. (1) can then be used as the basis for a number of computations, which we illustrate for quantum spin chain Hamiltonians. First we obtain the ground state energy E_{gs} and ground state wavefunction $|\Psi_{\text{gs}}\rangle$ of H ,

$$H|\Psi_{\text{gs}}\rangle = E_{\text{gs}}|\Psi_{\text{gs}}\rangle, \quad E_{\text{gs}} = \min_{|\Psi\rangle} \frac{\langle\Psi|H|\Psi\rangle}{\langle\Psi|\Psi\rangle}. \quad (2)$$

We then use the update (1) to simulate time evolution according to H ,

$$|\Psi(t)\rangle = e^{-itH} |\Psi(0)\rangle, \quad (3)$$

starting from some initial state $|\Psi(0)\rangle$. From the wavefunction $|\Psi\rangle$, one can compute all sorts of derived properties, such as correlation functions or entanglement measures, which we also illustrate.

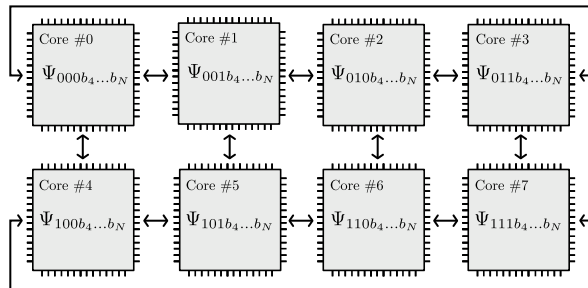
Tensor Processing Units.— TPUs come in boards. Each board holds 8 TPU cores controlled by a CPU host. Multiple boards can be joined together to form larger units, up to a so-called a pod, which for third generation TPUs consist of 2048 cores (that is, 256 boards). Each TPU v3 core has 16 GB of high bandwidth memory (HBM) attached to it, which amounts to 128 GB of HBM per board, or 32 TB per pod. Each TPU v3 core also has two matrix multiplication units (MXUs), which together deliver 52.5 teraFLOPS (floating-point operations per second) of matrix multiplication performance in half precision. MXUs natively perform matrix products by truncating single precision inputs to a half precision format called bfloat16, and accumulating the result again in single precision. Single precision matrix products are then achieved by composing six passes through the MXU (so the above FLOP counts can be divided by six to yield the equivalent single precision FLOPS). Finally, double precision is also available through software emulation with significant additional time and memory overheads [27].

A key aspect of TPUs, both in single-board and multi-board configurations, is that all the cores are directly connected to nearest neighbors in a toroidal mesh using fast ICIs and can therefore communicate without going through their CPU host(s). As a result, we observe multi-core performance scaling nearly linearly in the number of cores (e.g. 420 teraFLOPS per board, 100+ petaFLOPS per pod) even in tasks requiring significant communication between cores.

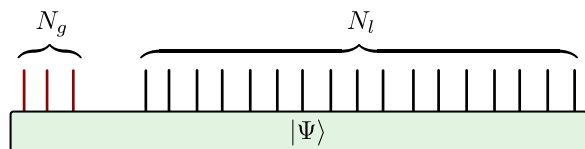
Code to run on TPUs can be written in several different frameworks, but we use the Python library Jax, which interfaces with the XLA just-in-time compiler [28, 29]. Parallelism between cores follows the single instruction multiple data (SIMD) paradigm. The HBM stores arrays in chunks of 8×128 , and the MXUs natively perform matrix products of 128×128 matrices. Care must be taken when writing code for TPUs to make sure arrays come in multiples of these sizes, to maintain high performance.

Wavefunction distribution.— Consider the wavefunction $|\Psi\rangle$ of N spin- $\frac{1}{2}$ quantum spins, or N qubits, characterized by the 2^N complex amplitudes $\Psi_{b_1 b_2 \dots b_N} = \langle b_1 b_2 \dots b_N | \Psi \rangle$. Each amplitude is indexed by a bit string (b_1, \dots, b_N) , where $b_i \in \{0, 1\}$, and stored here as a pair of single precision floating-point numbers for the real and imaginary parts. Assume that 2^{N_g} TPU cores are available. [For instance, a board has $2^3 = 8$ cores and thus $N_g = 3$, whereas a full pod has $2^{11} = 2048$ cores, or $N_g = 11$.] We divide the N qubits into two groups: the first N_g qubits and the remaining $N_l = N - N_g$ qubits, which are called *global* and *local* qubits, respectively. We also decompose each bit-string (b_1, \dots, b_N) into global and local pieces (b_1, \dots, b_{N_g}) and (b_{N_g+1}, \dots, b_N) . We then break the 2^N -element array $\Psi_{b_1 \dots b_{N_g} b_{N_g+1} \dots b_N}$ into 2^{N_g} sub-arrays of 2^{N_l} elements each, corresponding to the components with constant global bit-string (b_1, \dots, b_{N_g}) , and store each sub-array locally in the HBM of a single TPU core. For instance,

for a TPU board ($N_g = 3$) we would have 8 sub-arrays distributed over 8 cores, labelled #0 to #7, as follows:



We denote the distributed wavefunction with the following diagram, where each line corresponds to a qubit (red lines on the left correspond to global qubits):

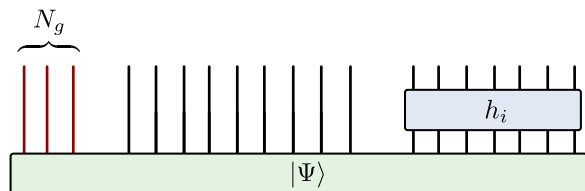


TPU memory considerations require that we store each local sub-array as an array with two or more dimensions, where the last two dimensions are multiples of 8 and 128 respectively, see App. A for more details.

Wavefunction update.— Consider now a local Hamiltonian $H = \sum_{i=1}^P h_i$ that decomposes as a sum of P local terms h_i , each acting on 7 qubits. We focus on 7-qubit terms because they fit the memory constraints of TPUs, see App. B for how to turn a more generic local Hamiltonian into this form. In order to apply H on $|\Psi\rangle$ as in Eq. (1), we compute a sequence of products $h_i |\Psi\rangle$ for $i = 1, \dots, P$, which we accumulate in wavefunctions $|\Psi^{(i)}\rangle$,

$$|\Psi^{(i)}\rangle = |\Psi^{(i-1)}\rangle + h_i |\Psi\rangle, \quad i = 1, \dots, P, \quad (4)$$

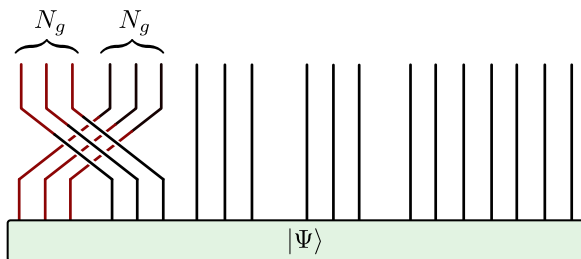
where $|\Psi^{(0)}\rangle = 0$ is the null vector and $|\Psi^{(P)}\rangle = H |\Psi\rangle$ contains the final result. Each Hamiltonian term h_i is represented by a $2^7 \times 2^7 = 128 \times 128$ matrix and broadcast to each TPU core. Assume first that the term h_i acts on the last 7 local qubits. We then simply multiply the distributed array for Ψ , regarded as a $2^{N-7} \times 2^7$ matrix, with the $2^7 \times 2^7$ matrix h_i , represented as:



This product is performed for each sub-array locally on each TPU core, utilizing the MXUs. When h_i acts on other local qubits, we can choose to permute their order so that h_i effectively acts on the last 7 local qubits.

This requires reshaping and/or transposing the local sub-array of Ψ on each core, while paying due attention to the restrictions on array shapes mentioned above (see also App. A). All the above operations are executed in parallel and without inter-core communication, with each core manipulating their local sub-array according to an identical set of instructions.

Finally, when the term h_i acts on at least one global qubit, we first re-distribute the wavefunction $|\Psi\rangle$, by swapping (possibly a subset of) the global qubits with an equivalent number of local qubits, in such a way that the Hamiltonian term h_i ends up acting on local qubits, at which point we can compute $h_i|\Psi\rangle$ as described above. For instance, in a single-board (i.e. 8-core) set-up, with $N_g = 3$, we may want to swap the three global qubits with the first three local qubits, represented by



The re-distribution of $|\Psi\rangle$, executed remarkably fast thanks to the ICIs, requires substantial communication between the cores. Fig. 1 shows the total time required for the update $|\Psi\rangle \mapsto H|\Psi\rangle$ for an example Hamiltonian. Using a full TPU v3 pod, the wavefunction for $N = 38$ qubits is updated in about 1 second.

Computation of ground states.— To illustrate the computation of a ground state $|\Psi_{gs}\rangle$, Eq. (2), we apply the Lanczos algorithm, based on the update $|\Psi\rangle \mapsto H|\Psi\rangle$ as described in App. D, to the 1D XXZ Hamiltonian,

$$H = J \sum_{i=1}^N (X_i X_{i+1} + Y_i Y_{i+1} + \Delta Z_i Z_{i+1}), \quad (5)$$

where X , Y , and Z are the Pauli matrices and site N is identified with site 0 (periodic boundary conditions). For the couplings $J = -1$ and $\Delta = \frac{1}{2}$, this model is known to be at a quantum critical point, in the universality class of a bosonic conformal field theory with unit central charge [31]. Our current implementation, which handles generic 1D local Hamiltonians, does not exploit any of the several symmetries of the XXZ model, e.g. translation invariance or internal $U(1)$ symmetry. The 2-qubit terms in the above Hamiltonian are merged together into 7-qubit terms (see App. B) to optimize the use of the MXUs. For this computation we use at most 128 TPU v3 cores ($N_g = 7$) to reach up to $N = 34$ qubits, with the total time for the computation being around 12 minutes.

Importantly, from the distributed array for $|\Psi\rangle$ we can extract a large variety of quantities, including e.g. wavefunction overlaps $\langle \Psi_1 | \Psi_2 \rangle$, expectation value of observables such as the energy $\langle \Psi | H | \Psi \rangle$, correlation func-

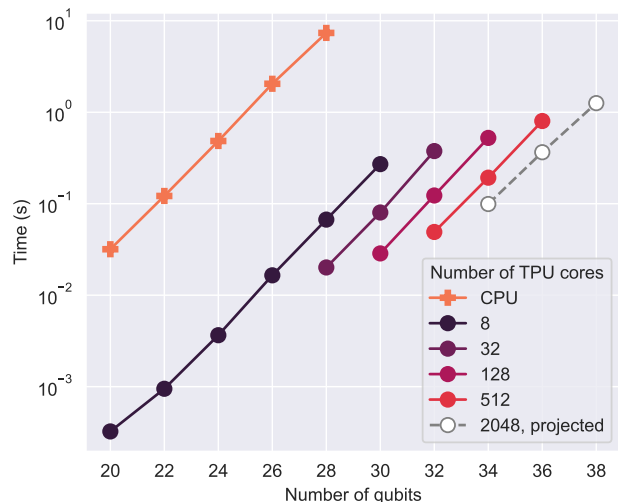


FIG. 1. Compute time for the update $|\Psi\rangle \mapsto H|\Psi\rangle$ for a 1D, nearest neighbor Hamiltonian such as that in Eq. 5, as a function of the number of qubits. Different colors represent different numbers of TPU cores, ranging from a single board (8 cores) to a full pod (2048 cores). Times are averaged over a large number of repetitions. Results for 2048 cores are extrapolated estimates, due to temporary resource constraints. CPU results were run on an 8-core 2.3GHz Intel Xeon workstation, using a Numba-based [30] implementation. They represent a typical workstation, rather than cutting-edge high-performance computing hardware.

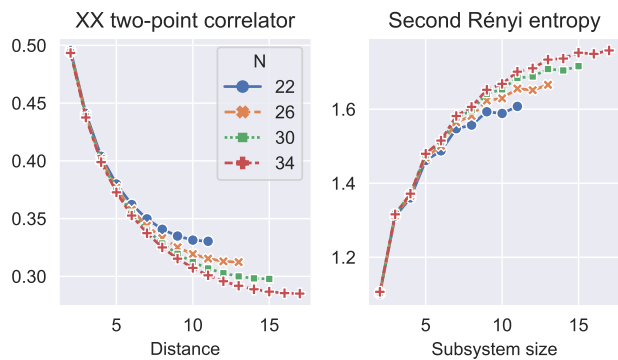


FIG. 2. Properties of the ground state of the 1D XXZ model in Eq. (5) with $J = -1$, $\Delta = \frac{1}{2}$. Left: The $\langle X_1 X_n \rangle - \langle X_1 \rangle \langle X_n \rangle$ connected two-point correlator as a function of the distance n . Right: Second Rényi entropy S_2 of a subsystem as a function of subsystem size. The different lines are for different system sizes.

tions and entanglement measures. This requires additional operations that can also be easily implemented on TPUs. The reduced density matrix $\rho_A = \text{Tr}_{\bar{A}} |\Psi\rangle \langle \Psi|$ over a subset A of qubits (where the trace is over the rest of the qubits, denoted \bar{A}), and derived quantities such as von Neumann and Rényi entropies can also be computed for subsystems of up to $N/2$ qubits. Handling them requires distributed linear algebra meth-

ods on TPUs, discussed in Ref. 19. As an example, Fig. 2 shows the connected two-point correlator $\langle \Psi | X_1 X_n | \Psi \rangle - \langle \Psi | X_1 | \Psi \rangle \langle \Psi | X_n | \Psi \rangle$ as a function of the distance n between spins, as well as the second Rényi entropy $S_2(\rho_A) = -\log_2 \text{Tr}[(\rho_A)^2]$, where ρ_A corresponds to a subsystem A of contiguous spins.

Simulation of time evolution.— Our second application is the simulation of a time evolution $|\Psi(t)\rangle = e^{-itH} |\Psi(0)\rangle$ that generates large amounts of entanglement. We define a suitably small time interval δt such that $q \equiv t/\delta t$ is an integer, write the time evolution operator for time t , $\exp(-itH)$, as the q -fold product of the time operator for δt , $\exp(-itH) = \prod_{j=1}^q \exp(-i\delta t H)$, and then approximate each operator $\exp(-i\delta t H)$ as a sequence of six terms of the form $(1 - ia_n \delta t H)$,

$$\begin{aligned} \exp(-i\delta t H) &= (1 - ia_6 \delta t H) \times \dots \\ &\dots \times (1 - ia_2 \delta t H) \times (1 - ia_1 \delta t H) + O(\delta t^7), \end{aligned} \quad (6)$$

where the coefficients a_n are solved for numerically, see App. C. The dominant term neglected above is $\frac{H^7 \delta t^7}{7!}$. Each update $|\Psi\rangle \mapsto (1 - ia_n \delta t H) |\Psi\rangle$ requires computing $|\Psi\rangle \mapsto H |\Psi\rangle$ and is implemented while keeping only a few copies of $|\Psi\rangle$ in memory simultaneously.

For this demonstration we choose a 1D local Hamiltonian of the form $H = \sum_{i=1}^N h_{[i,i+5]}$, where each $h_{[i,i+5]}$ is a Hermitian matrix of size $2^6 \times 2^6$ that operates on qubits i through $i+5$, thus exemplifying the use of k -qubit Hamiltonian terms for $k > 2$. H is set to have periodic boundaries. The matrix elements of $h_{[i,i+5]}$, which represents a generic non-integrable many-body interaction, are Gaussian distributed with mean zero and standard deviation $\sqrt{6} 2^{-5}$ (such that the average Frobenius norm of each term is $\langle \|h_{[i,i+5]}\| \rangle = \sqrt{6}$). The 6-qubit terms $h_{[i,i+5]}$ are still pairwise blocked into 7-qubit terms (see App. B) in order to optimally utilize the MXUs.

Fig. 3 shows the second Rényi entropy, as a function of time t , of various subsystems for the state $|\Psi(t)\rangle = \exp(-itH) |\Psi(0)\rangle$, where the initial state $|\Psi(0)\rangle$ has no entanglement, and the system has $N = 32$ qubits. On 32 TPU v3 cores ($N_g = 5$), simulating this evolution, which includes $q = 500$ time steps with $\delta t = 0.02$, and evaluation of the entropies, took 44 minutes. At early times the entropy is seen to grow similarly for all subsystems, regardless of their size. However, in time each subsystem saturates to a constant amount of entropy, dependent only on the size of the subsystem. Specifically, for a subsystem of M qubits this saturation value is roughly M bits of entropy, except for subsystems that cover a large proportion of the total system, such as $M = \frac{N}{2}$, for which it is somewhat less, as expected [32]. For the larger subsystems we see a sustained period of linear growth, which is evidence for ballistic growth of entanglement, as expected for a random Hamiltonian [33]. The rapid growth of entanglement all the way to saturation makes this time evolution very hard to simulate using tensor network methods such as Matrix Product States (MPS), which rely on the wavefunction being only moderately entangled and thus compressible. Indeed, in

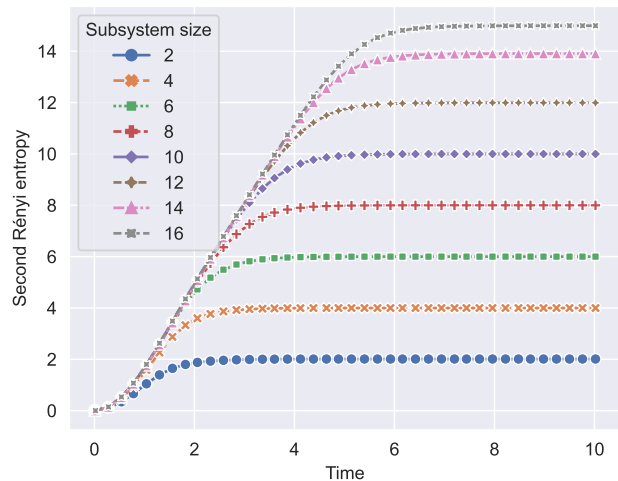


FIG. 3. Second Rényi entropy S_2 of various subsystems, as a function of time t , during an entangling time evolution $|\Psi(t)\rangle = e^{-itH} |\Psi(0)\rangle$ on $N = 32$ qubits, starting from an unentangled product state $|\Psi(0)\rangle$ and according to a 1D random Hamiltonian with 6-qubit terms. For each subsystem size, the entropy initially grows until saturating to a maximum value corresponding to a random wavefunction.

this example an MPS description would require a central bond dimension close to $2^{16} = 65,536$. In other words, the largest MPS tensors have a similar size as the whole wavefunction (2^{32} complex coefficients), making the MPS approach even more costly than the present brute-force approach.

Discussion.— TPUs, originally designed for machine learning workloads, can be effectively repurposed to accelerate and scale up a number of other computationally demanding tasks [12–26]. In this paper we have demonstrated that TPUs can be used to compute ground states and simulate real time evolution in many-body systems. A very high matrix multiplication throughput on each core (enabled by the MXUs), combined with the ability to directly connect up to thousands of TPU cores together (using the fast ICIs) for a single parallel simulation with dozens of terabytes of HBM allowed us to consider an unusually large number N of qubits at remarkable speed, see e.g. Fig. 1. This required adjusting to a number of characteristic features of TPUs and their XLA compiler, such as operating under the SIMD paradigm and using specific shapes for the matrices and arrays. Importantly, operating with k -qubit Hamiltonian terms for $k < 7$ has a computational cost similar to the $k = 7$ case, for which we observe peak performance.

Here we have considered local Hamiltonians H in one dimension for concreteness. It is of course also possible to address 2D/3D local Hamiltonians, e.g. for square/cubic lattices, where sizes 6×6 , 4×9 or $4 \times 3 \times 3$ are easily accessible. To go well beyond these system sizes, one has to give up a brute-force, exact simulation based on storing the full wavefunction, and use instead approximate methods such as tensor network ap-

proaches. Tensor network methods can also be significantly accelerated and scaled up with TPUs, allowing e.g. for MPS representations of 100-qubit wavefunctions with unusually large bond dimensions [25], capable of describing larger amounts of entanglement than it is possible on regular hardware.

ACKNOWLEDGMENTS

This research was supported with Cloud TPUs from Google’s TPU Research Cloud (TRC). Sandbox is a team within the Alphabet family of companies, which includes Google, Verily, Waymo, X, and others. GV is a CIFAR fellow in the Quantum Information Science Program and a Distinguished Visiting Research Chair at Perimeter Institute. Research at Perimeter Institute is supported by the Government of Canada through the Department of Innovation, Science and Economic Development and by the Province of Ontario through the Ministry of Research, Innovation and Science.

-
- [1] H. G. Evertz, “The loop algorithm,” *Advances in Physics* **52**, 1–66 (2003), [arXiv:cond-mat/9707221](#).
- [2] N. V. Prokof’ev, B. V. Svistunov, and I. S. Tupitsyn, “Exact, complete, and universal continuous-time worldline Monte Carlo approach to the statistics of discrete quantum systems,” *Journal of Experimental and Theoretical Physics* **87**, 310–321 (1998), [arXiv:cond-mat/9703200](#).
- [3] Olav F. Syljuåsen and Anders W. Sandvik, “Quantum Monte Carlo with directed loops,” *Phys. Rev. E* **66**, 046701 (2002), [arXiv:cond-mat/0202316](#).
- [4] Steven R. White, “Density matrix formulation for quantum renormalization groups,” *Phys. Rev. Lett.* **69**, 2863–2866 (1992).
- [5] Guifré Vidal, “Efficient simulation of one-dimensional quantum many-body systems,” *Phys. Rev. Lett.* **93**, 040502 (2004).
- [6] F. Verstraete and J. I. Cirac, “Renormalization algorithms for quantum-many body systems in two and higher dimensions,” (2004), [arXiv:cond-mat/0407066](#).
- [7] G. Vidal, “A class of quantum many-body states that can be efficiently simulated,” *Phys. Rev. Lett.* **101**, 110501 (2008), [arXiv:quant-ph/0610099](#).
- [8] Michael Levin and Cody P. Nave, “Tensor renormalization group approach to 2D classical lattice models,” *Phys. Rev. Lett.* **99**, 120601 (2007), [arXiv:cond-mat/0611687](#).
- [9] Jutho Haegeman, J. Ignacio Cirac, Tobias J. Osborne, Iztok Pizorn, Henri Verschelde, and Frank Verstraete, “Time-dependent variational principle for quantum lattices,” *Phys. Rev. Lett.* **107** (2011), [arXiv:1103.0936](#).
- [10] Norman Jouppi, Doe Yoon, George Kurian, Sheng Li, Nishant Patil, James Laudon, Cliff Young, and David Patterson, “A domain-specific supercomputer for training deep neural networks,” *Communications of the ACM* **63**, 67–78 (2020).
- [11] Norman P. Jouppi, Cliff Young, Nishant Patil, David Patterson, Gaurav Agrawal, Raminder Bajwa, Sarah Bates, Suresh Bhatia, Nan Boden, Al Borchers, *et al.*, “In-datacenter performance analysis of a tensor processing unit,” in *Proceedings of the 44th Annual International Symposium on Computer Architecture*, ISCA ’17 (Association for Computing Machinery, New York, NY, USA, 2017) p. 1–12.
- [12] Francois Belletti, Davis King, Kun Yang, Roland Nelet, Yusef Shafi, Yi-Fan Chen, and John Anderson, “Tensor processing units for financial Monte Carlo,” (2020), [arXiv:1906.02818 \[cs.DC\]](#).
- [13] Qing Wang, Matthias Ihme, Yi-Fan Chen, and John Anderson, “A tensorflow simulation framework for scientific computing of fluid flows on tensor processing units,” (2021), [arXiv:2108.11076 \[physics.comp-ph\]](#).
- [14] Zhixin Pan and Prabhat Mishra, “Hardware acceleration of explainable machine learning using tensor processing units,” (2021), [arXiv:2103.11927 \[cs.LG\]](#).
- [15] Tianjian Lu, Thibault Marin, Yue Zhuo, Yi-Fan Chen, and Chao Ma, “Accelerating MRI reconstruction on TPUs,” (2020), [arXiv:2006.14080 \[cs.CE\]](#).
- [16] Chao Ma, Thibault Marin, T.J Lu, Yi fan Chen, and Yue Zhuo, “Nonuniform fast fourier transform on TPUs,” (2021).
- [17] Tianjian Lu, Yi-Fan Chen, Blake Hechtman, Tao Wang, and John Anderson, “Large-scale discrete fourier transform on TPUs,” (2020), [arXiv:2002.03260 \[cs.MS\]](#).
- [18] Fantine Huot, Yi-Fan Chen, Robert Clapp, Carlos Boneti, and John Anderson, “High-resolution imaging on TPUs,” (2019), [arXiv:1912.08063 \[cs.CE\]](#).
- [19] Adam G. M. Lewis et al., “Tensor Processing Units for Distributed Dense Linear Algebra,” Sandbox@Alphabet, *in preparation*.
- [20] Martin Ganahl et al., “Tensor Processing Units for Simulating Quantum Circuits,” Sandbox@Alphabet, *in preparation*.
- [21] Alan Morningstar, Markus Hauru, Jackson Beall, Martin Ganahl, Adam G. M. Lewis, Vedika Khemani, and Guifre Vidal, “Simulation of quantum many-body dynamics with Tensor Processing Units: Floquet prethermalization,” Sandbox@Alphabet, *in preparation*.
- [22] Ross Shillito, Alexandru Petrescu, Joachim Cohen, Jackson Beall, Markus Hauru, Martin Ganahl, Adam G. M. Lewis, Alexandre Blais, and Guifre Vidal, “Classical simulation of superconducting quantum hardware using Tensor Processing Units,” Sandbox@Alphabet, *in preparation*.
- [23] Ryan Pederson et al., “Tensor Processing Units for Quantum Chemistry,” Sandbox@Alphabet, *in preparation*.
- [24] Ruyi Song et al., “Simulation of Spin Light Emitting Diodes using Tensor Processing Units,” Sandbox@Alphabet, *in preparation*.
- [25] Martin Ganahl et al., “Density Matrix Renormalization Group using Tensor Processing Units,” Sand-

- box@Alphabet, *in preparation*.
- [26] Erik Gustafson, Burt Holzman, James Kowalkowski, Henry Lamm, Andy C. Y. Li, Gabriel Perdue, Sergio Boixo, Sergei Isakov, Orion Martin, Ross Thomson, *et al.*, “Large scale multi-node simulations of \mathbb{Z}_2 gauge theory quantum circuits using google cloud platform,” (2021), [arXiv:2110.07482](https://arxiv.org/abs/2110.07482) [quant-ph].
- [27] All the results presented in this paper correspond to end-to-end computations conducted in single precision. This is in contrast with the double precision often used in scientific computing. Our numerical experiments confirmed that single precision, capable of roughly 7 digits of accuracy, was sufficient to yield stable, numerically precise results. This is consistent with the error accumulation analysis of Ref. 21, where very deep quantum circuits, with several millions of gates, were successfully simulated using single precision.
- [28] James Bradbury, Roy Frostig, Peter Hawkins, Matthew James Johnson, Chris Leary, Dougal Maclaurin, George Necula, Adam Paszke, Jake VanderPlas, Skye Wanderman-Milne, and Qiao Zhang, “JAX: composable transformations of Python+NumPy programs,” (2018).
- [29] <https://tensorflow.org/xla>, accessed: 2021-10-01.
- [30] Siu Kwan Lam, Antoine Pitrou, and Stanley Seibert, “Numba: A llvm-based python jit compiler,” in *Proceedings of the Second Workshop on the LLVM Compiler Infrastructure in HPC*, LLVM ’15 (Association for Computing Machinery, New York, NY, USA, 2015).
- [31] Malte Henkel, *Conformal Invariance and Critical Phenomena* (Springer, Berlin, Heidelberg, 1999).
- [32] Patrick Hayden, Debbie Leung, and Andreas Winter, “Aspects of generic entanglement,” *Communications in Mathematical Physics* **265**, 95–117 (2006).
- [33] Hyungwon Kim and David A. Huse, “Ballistic spreading of entanglement in a diffusive nonintegrable system,” *Phys. Rev. Lett.* **111**, 127205 (2013), [arXiv:1306.4306](https://arxiv.org/abs/1306.4306).

Appendix A: Distribution and manipulation of an N -qubit wavefunction on TPUs

Consider the wavefunction $|\Psi\rangle$ of a system of N qubits,

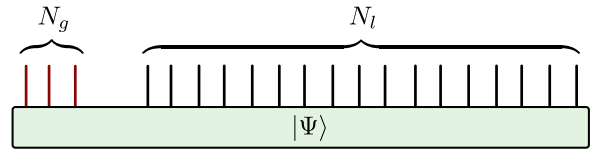
$$|\Psi\rangle = \sum_{b_1=0}^1 \sum_{b_2=0}^1 \cdots \sum_{b_N=0}^1 \Psi_{b_1 b_2 \dots b_N} |b_1 b_2 \dots b_N\rangle, \quad (\text{A1})$$

which is characterized by 2^N complex amplitudes $\Psi_{b_1 b_2 \dots b_N} = \langle b_1 b_2 \dots b_N | \Psi \rangle$. In this appendix we explain how to distribute the 2^N amplitudes $\Psi_{b_1 b_2 \dots b_N}$ over a number 2^{N_g} of TPU cores. We also explain how to update the distributed wavefunction under the action of a 7-qubit operator h , $|\Psi\rangle \mapsto h|\Psi\rangle$.

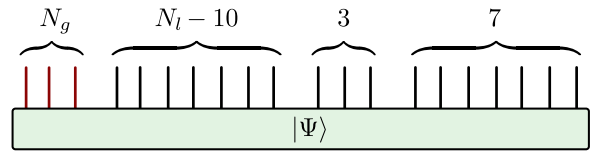
We index each amplitude $\Psi_{b_1 b_2 \dots b_N}$ by a bit-string (b_1, \dots, b_N) , where $b_i \in \{0, 1\}$, corresponding to the computational basis vector $|b_1 b_2 \dots b_N\rangle$. We then divide the N qubits into two groups. The first group contains N_g qubits, which we call *global* qubits. The second group contains the remaining $N_l = N - N_g$ qubits, referred to as *local* qubits. Accordingly, each bit-string (b_1, \dots, b_N) is divided into a global part (b_1, \dots, b_{N_g}) and local part (b_{N_g+1}, \dots, b_N) . The global part (b_1, \dots, b_{N_g})

determines the TPU core where the amplitude is stored. For instance, for $N_g = 3$ we have 8 cores, labelled $\{(000), (001), (010), \dots, (111)\}$, and core (000) stores the amplitudes $\Psi_{000b_4 \dots b_N}$, core (001) stores the amplitudes $\Psi_{001b_4 \dots b_N}$, etc. In this way, core (c_1, \dots, c_{N_g}) (where we temporarily label the global part of the bit-string using c 's to emphasize that they are constant on a given core) stores the 2^{N_l} -element sub-array $\Psi_{c_1 \dots c_{N_g} b_{N_g+1} \dots b_N}$ with components labelled by the local bit-string (b_{N_g+1}, \dots, b_N) corresponding to the local qubits.

In other words, we think of the 2^N amplitudes $\Psi_{b_1 b_2 \dots b_N}$ of a single distributed array as 2^{N_g} sub-arrays of size 2^{N_l} , each one stored locally on the corresponding TPU core. Graphically we denote this with the following diagram, where the lines denote qubits with the red ones on the left being the global ones:



Data in TPU memory is stored in chunks of size 8×128 . This means that, for any array, the last two indices must have sizes that are multiples of 8 and 128 (otherwise the array will be padded with zeros until it has that shape, incurring a waste of memory that should be avoided). Given that $2^3 = 8$ and $2^7 = 128$, this corresponds to using the last two indices of the array to label at least 3 and 7 qubits, respectively. We thus store the wavefunction using a distributed array with a shape that adjusts to this rule. For instance, with the shape $(2^{N_g}, 2^{N_l-10}, 2^3, 2^7)$, that is, where each local sub-array on each core has shape $(2^{N_l-10}, 2^3, 2^7)$. Graphically:



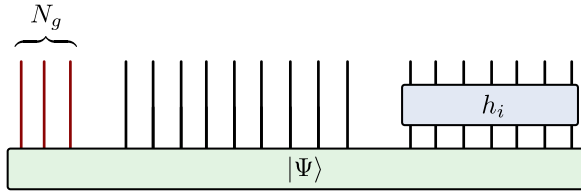
Our next step is to consider the update $|\Psi\rangle \mapsto h|\Psi\rangle$, where h represents a 7-qubit operator, or a matrix with shape $(128, 128)$, which we broadcast so that each core holds a copy. Let us label the components $h_{\vec{\alpha}\vec{\alpha}'}$ of this matrix by indices $\vec{\alpha}$ resulting from composing 7 binary indices, $\vec{\alpha} = (\alpha_1, \alpha_2, \dots, \alpha_7)$, with $\alpha_i \in \{0, 1\}$. We next consider three cases, depending on which qubits the 7-qubit operator h acts on.

(i) First we assume that h acts on the last 7 local qubits. We can then simply multiply h and the local $|\Psi\rangle$ together by contracting over the last index of the local sub-array,

$$\Psi_{c_1 \dots c_{N_g} b_{N_g+1} \dots b_{N-7} \vec{\alpha}} \mapsto \quad (\text{A2})$$

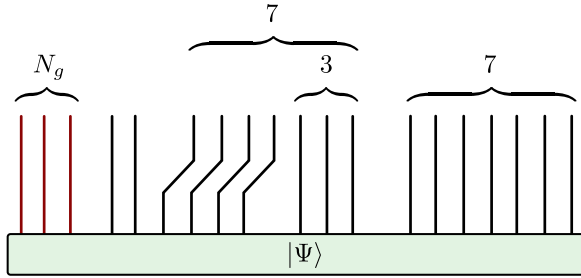
$$\sum_{\vec{\alpha}'} h_{\vec{\alpha}, \vec{\alpha}'} \Psi_{c_1 \dots c_{N_g} b_{N_g+1} \dots b_{N-7} \vec{\alpha}'} \quad (\text{A3})$$

Graphically this can be represented as

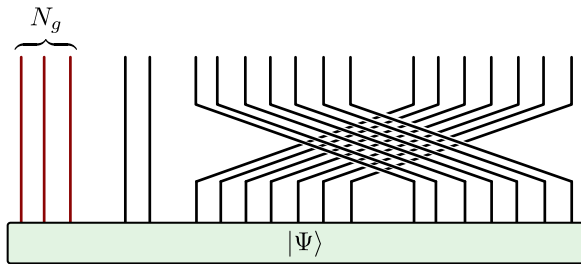


Importantly, this update of the distributed wavefunction can be accomplished by having each TPU core update its corresponding local sub-array, so that the 2^{N_g} local sub-arrays are updated in parallel without need for inter-core communication.

(ii) Next we assume that the 7-qubit gate acts on arbitrary local qubits, and not just the last 7 qubits as before. In this case, we re-organize each of the local sub-arrays so as to move the 7 targeted qubits to the last 7 positions, followed by the above contraction, and then by the reversal of the above re-organization. The re-organization of a local sub-array consists of a sequence of reshapes and transpositions. For instance, we could reshape the local sub-array from shape $(2^6, 2^3, 2^7)$ to shape $(2^2, 2^7, 2^7)$, represented by



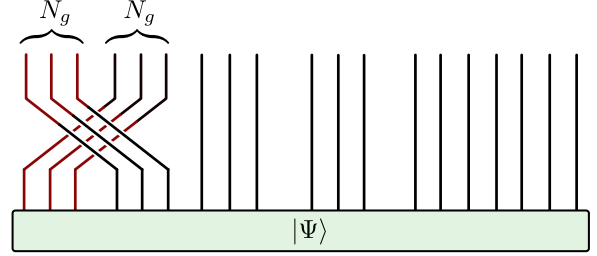
and then transpose the two last indices of the resulting local sub-array, which we draw as



Notice that at each step of this example, we store a local array where the range of the last two indices correspond to, at least, 3 and 7 qubits, respectively (that is, to multiples of 8 and 128), so as to prevent padding with zeros. Once again, all these operations are performed in parallel without need for inter-core communication.

(iii) Finally, to apply the update $|\Psi\rangle \mapsto h|\Psi\rangle$ when h acts on a set of qubits that includes at least one of the global qubits, we first re-distribute the wavefunction so that all the targeted qubits become local, then proceed as

above, and then re-distribute the resulting wavefunction back to the original form. For instance, if $N_g = 3$ and h acts on the three global qubits, but not on the first three local qubits, we can re-distribute the wavefunction by swapping the global qubits with the first three local qubits, represented as



Notice that this transformation cannot be performed locally on each TPU core, but requires instead substantial communication between the cores. TPUs can perform such inter-core communication remarkably fast, thanks to the dedicated ICIs that connects the cores directly, bypassing the CPU hosts on each TPU board.

Appendix B: Local Hamiltonian

As discussed in the main text, TPUs natively do matrix products of size 128×128 , or $2^7 \times 2^7$. In this Appendix we explain how to use this ability to compute the update $|\Psi\rangle \mapsto H|\Psi\rangle$ for a local Hamiltonian H that decomposes as a sum of local terms.

Consider a local Hamiltonian

$$H = \sum_{i=1}^Q k_i \quad (\text{B1})$$

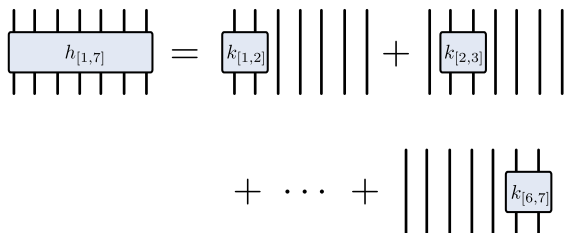
where each of the Q terms k_i is an operator that acts non-trivially on at most 7 qubits, possibly less. Recall that on a TPU, a matrix multiplication involving matrices with dimensions less than 128×128 is done by padding the matrices with zeros until they are of size 128×128 . That means that we would like to be working with local terms h_i that act on exactly 7 qubits, not less. Accordingly, our first goal is to rewrite the above Hamiltonian as

$$H = \sum_{i=1}^P h_i \quad (\text{B2})$$

where each 7-qubit term h_i may come from adding two or more terms k_i in Eq. (B1). As an example, consider a 1D local Hamiltonian where each term k_i acts on two consecutive qubits, denoted $k_{[i, i+1]}$. Then we define the 7-qubit terms h_i , denoted $h_{[i, i+6]}$, by adding together 6 of such terms. For instance, the first 7-qubit operator reads

$$h_{[1,7]} = k_{[1,2]} \otimes \mathbb{1}_5 + \mathbb{1}_1 \otimes k_{[2,3]} \otimes \mathbb{1}_4 + \mathbb{1}_2 \otimes k_{[3,4]} \otimes \mathbb{1}_3 + \dots + \mathbb{1}_5 \otimes k_{[6,7]}. \quad (\text{B3})$$

Here $\mathbb{1}_m$ is the identity on m qubits. Graphically we represent this as



We can similarly define $h_{[7,13]}$, $h_{[13,19]}$, etc. Notice that, in this example, if e.g. $N = 22$, the last term $h_{[19,22]}$ only acts on 4 qubits. In that case, we will tensor product $h_{[19,22]}$ with the identity $\mathbb{1}_3$ on 3 additional qubits, into a 7-qubit operator $h_{[16,22]} = \mathbb{1}_3 \otimes h_{[19,22]}$.

To compute $|\Psi\rangle \mapsto H|\Psi\rangle$ for $H = \sum_i h_i$, we compute a sequence of products $h_i|\Psi\rangle$ for $i = 1, \dots, P$, which we accumulate in wavefunctions $|\Psi^{(i)}\rangle$,

$$|\Psi^{(i)}\rangle = |\Psi^{(i-1)}\rangle + h_i|\Psi\rangle, \quad i = 1, \dots, P, \quad (\text{B4})$$

where $|\Psi^{(0)}\rangle = 0$ is the null vector and $|\Psi^{(P)}\rangle = H|\Psi\rangle$ contains the final result. Notice that during the above steps we need to keep at least three distributed arrays on the TPUs, corresponding to wavefunctions Ψ , $h_i|\Psi\rangle$ and $|\Psi^{(i-1)}\rangle$.

It is instructive to evaluate what the loss in efficiency is if we disregard the rule that matrix products should involve a matrices of shape $(2^7, 2^7) = (128, 128)$ (or, more generally, multiples of these dimensions). Suppose, as a concrete example, that our goal is to multiply the 2^N -element distributed array for an N -qubit wavefunction $|\Psi\rangle$ [properly reshaped into a matrix with shape $(2^{N-2}, 2^2)$] by a two-qubit term k [or matrix with shape $(2^2, 2^2)$]. On a CPU, this matrix product would require roughly $2^{N-2} \times 2^2 \times 2^2 = 2^{N+2}$ floating-point multiplications (and a similar number of additions, which we ignore in our counting for simplicity). On a TPU, we first need to pad both matrices with zeros until they reach shapes $(2^{N-2}, 2^7)$ and $(2^7, 2^7)$, respectively. We see that storing the wavefunction in this format requires the same memory as $2^5 = 32$ copies of $|\Psi\rangle$ stored without padding. For large N , this is a massive waste of memory! In addition, the matrix multiplication now requires $2^{N-2} \times 2^7 \times 2^7 = 2^{N+12}$ floating-point multiplications, which is $2^{10} = 1024\times$ more than on a CPU! Again, a massive waste of compute time.

Given the constraints forced on us by the MXU, how can we more efficiently accomplish the above product? We proceed by augmenting the two-qubit operator k into a 7-qubit operator h , given by $h = k \otimes \mathbb{1}_5$, that acts as the identity on 5 additional qubits. We then reshape the 2^N -element array into a matrix of shape $(2^{N-7}, 2^7)$ and multiply it by the $(2^7, 2^7)$ -shaped matrix for h . Notice that no padding with zeros is now required. In addition, the matrix multiplication now requires roughly $2^{N-7} \times 2^7 \times 2^7 = 2^{N+7}$ floating-point operations, which is $2^5 = 32\times$ more the operations needed on a CPU (still a

very significant waste, but better than the factor $1024\times$). In addition, If we can join the two-qubit term k with other two-qubit terms that are also part of the same Hamiltonian, we can include them in the same matrix multiplication. For instance, in Eq. (B3) we joined 6 two-qubit terms into a single seven-qubit term. In that case the MXU forces us into a factor $32/6 \approx 5.3\times$ more operations compared to a CPU. Needless to say, the extreme efficiency of the MXU by far compensates for the generation of additional floating-point operations. Finally, we remark that for 7-qubit operators (or operators acting on even a larger number of qubits), the MXU does not force us into generating additional floating-point operations, achieving its optimal efficiency.

Appendix C: Expansion of the time evolution operator

To numerically time evolve a quantum state, we take the time evolution operator for a small time δt , $\exp(-i\delta t H)$, and Taylor expand the exponential to sixth order:

$$\exp x = \sum_{n=0}^6 \frac{1}{n!} x^n + O(x^7) = \prod_{n=1}^6 (1 + a_n x) + O(x^7) \quad (\text{C1})$$

The latter form is nothing but a rewriting of the polynomial $\sum_{n=0}^6 \frac{1}{n!} x^n$ in terms of its roots a_n , which can be solved for numerically. To accuracy sufficient for single precision, the roots are

$$\begin{aligned} a_1 &= 0.37602583 - 0.13347447i, & a_2 &= a_1^*, \\ a_3 &= -0.05612287 - 0.25824122i, & a_4 &= a_3^*, \\ a_5 &= 0.18009704 + 0.30409897i, & a_6 &= a_5^*, \end{aligned}$$

Appendix D: Memory efficient Lanczos algorithm

The Lanczos method is a matrix-free diagonalization technique which can be used to approximate extremal (largest in magnitude) eigenvector-eigenvalue pairs of a large Hermitian linear operator H . The only requirements (besides H being Hermitian) is the ability to efficiently compute the action of H on a given vector \mathbf{x} , and enough memory to store at least four such vectors (plus some small amount of extra memory to perform auxiliary computations).

Algorithm 1 outlines the basic Lanczos method. Starting from a normalized initial guess \mathbf{x} for an extremal eigenstate of H , the Lanczos method iteratively builds an orthogonal basis $Q_j \equiv [\mathbf{x}_0, \mathbf{x}_1, \dots, \mathbf{x}_j]$ of Krylov vectors \mathbf{x}_n for the Krylov-subspace $\text{span}\{\mathbf{x}, H\mathbf{x}, \dots, H^j\mathbf{x}\}$. The algorithm makes explicit use of the Hermiticity of H to obtain the orthogonal basis Q_j through a three-step recurrence relation which at any point involves only

Algorithm 1 Lanczos algorithm

```

1: function LANCZOS( $H, \mathbf{x}, K, \delta$ )
2:    $\mathbf{x}_{-1} = \text{zeros\_like}(\mathbf{x})$ 
3:    $\mathbf{x}_0 = \mathbf{x}$ 
4:    $Q_{-1} = []$ 
5:   for  $n=0 \dots K-1$  do
6:      $\beta_n = \|\mathbf{x}_n\|$ 
7:     if  $\beta_n < \delta$  then ▷ invariant subspace found
8:       return  $\{\alpha_0, \dots, \alpha_{n-1}\}, \{\beta_0, \dots, \beta_n\}, Q_{n-1}$ 
9:     end if
10:     $\mathbf{x}_n \leftarrow \mathbf{x}_n / \beta_n$ 
11:     $Q_n = [Q_{n-1}, \mathbf{x}_n]$ 
12:     $\mathbf{x}_{n+1} = A\mathbf{x}_n$ 
13:     $\alpha_n = \langle \mathbf{x}_{n+1}, \mathbf{x}_n \rangle$  ▷  $\alpha_n \in \mathbb{R}$ 
14:     $\mathbf{x}_{n+1} \leftarrow \mathbf{x}_{n+1} - \alpha_n \mathbf{x}_n - \beta_n \mathbf{x}_{n-1}$ 
15:  end for
16:  return  $\{\alpha_0, \dots, \alpha_{K-1}\}, \{\beta_0, \dots, \beta_K\}, Q_{n-1}$ 
17: end function

```

Algorithm 2 Lanczos algorithm for computing a tri-diagonalization of H

```

1: function LANCZOS_TRIDIAG( $H, \mathbf{x}, K, \delta$ )
2:    $\mathbf{x}_{-1} = \text{zeros\_like}(\mathbf{x})$ 
3:    $\mathbf{x}_0 = \mathbf{x}$ 
4:   for  $n=0 \dots K-1$  do
5:      $\beta_n = \|\mathbf{x}_0\|$ 
6:     if  $\beta_n < \delta$  then ▷ invariant subspace found
7:       return  $\{\alpha_0, \dots, \alpha_{n-1}\}, \{\beta_0, \dots, \beta_n\}$ 
8:     end if
9:      $\mathbf{x}_0 \leftarrow \mathbf{x}_0 / \beta_n$ 
10:     $\mathbf{x}_1 = A\mathbf{x}_0$ 
11:     $\alpha_n = \langle \mathbf{x}_1, \mathbf{x}_0 \rangle$  ▷  $\alpha_n \in \mathbb{R}$ 
12:     $\mathbf{x}_1 \leftarrow \mathbf{x}_1 - \alpha_n \mathbf{x}_0 - \beta_n \mathbf{x}_{-1}$ 
13:     $\mathbf{x}_{-1} \leftarrow \mathbf{x}_0$ 
14:     $\mathbf{x}_0 \leftarrow \mathbf{x}_1$ 
15:  end for
16:  return  $\{\alpha_0, \dots, \alpha_{K-1}\}, \{\beta_0, \dots, \beta_K\}$ 
17: end function

```

Algorithm 3 Lanczos algorithm for computing an approximate ground state of H

```

1: function LANCZOS_GROUNDSTATE( $H, \mathbf{x}, \{\alpha_i\}, \{\beta_i\}, \{v_i\}$ )
2:    $\mathbf{u} = \text{zeros\_like}(\mathbf{x})$ 
3:    $\mathbf{x}_{-1} = \text{zeros\_like}(\mathbf{x})$ 
4:    $\mathbf{x}_0 = \mathbf{x}$ 
5:   for  $n=0 \dots \text{len}(\{v_i\})$  do
6:      $\mathbf{x}_0 \leftarrow \mathbf{x}_0 / \beta_n$ 
7:      $\mathbf{u} \leftarrow \mathbf{u} + v_n \mathbf{x}_0$ 
8:      $\mathbf{x}_1 = A\mathbf{x}_0$ 
9:      $\mathbf{x}_1 \leftarrow \mathbf{x}_1 - \alpha_n \mathbf{x}_0 - \beta_n \mathbf{x}_{-1}$ 
10:     $\mathbf{x}_{-1} \leftarrow \mathbf{x}_0$ 
11:     $\mathbf{x}_0 \leftarrow \mathbf{x}_1$ 
12:  end for
13:  return  $\mathbf{u}$ 
14: end function

```

three consecutive Krylov vectors. The Lanczos method converges towards the *dominant* eigenstate, i.e. the one with largest-in-magnitude eigenvalue, or a random linear superposition of states if the eigenvalue is degenerate. To achieve convergence towards the (algebraic) lowest eigenstate, one can e.g. apply a uniform spectral shift to H . The algorithm produces the real coefficients $\{\alpha_n\}, \{\beta_n\}$ of the tridiagonal matrix T_j ,

$$T_j \equiv \begin{pmatrix} \alpha_0 & \beta_1 & & & \\ \beta_1 & \alpha_1 & \beta_2 & & \\ & \beta_2 & \alpha_2 & \ddots & \\ & & \ddots & \ddots & \beta_j \\ & & & & \beta_j & \alpha_j \end{pmatrix} \quad (\text{D1})$$

with j at most equal to $K - 1$, where K is the Krylov space dimension chosen by the user, but smaller if the algorithm terminates early (see below). The matrices Q_j, T_j and H satisfy the Lanczos relation

$$HQ_j = Q_j T_j + \beta_{j+1} \mathbf{x}_{j+1} \mathbf{e}_{j+1}^T \quad (\text{D2})$$

with \mathbf{e}_{j+1} the $j+1$ -st euclidean basis-vector of dimension $j+1$. The algorithm terminates early if an invariant subspace is found, i.e. if a newly generated Krylov vector \mathbf{x}_n is a linear superposition of previous Krylov vectors. In this case the eigenvalues of T_j and the corresponding Ritz vectors (see below) are exact eigenvalues and eigenvectors of H . Given an eigenvector \mathbf{v} of T_j to eigenvalue λ , the corresponding Ritz vector \mathbf{u} is obtained by expanding \mathbf{v} in the Krylov basis Q_j :

$$\mathbf{u} = Q_j \mathbf{v}. \quad (\text{D3})$$

The pair (λ, \mathbf{u}) is called a Ritz pair. If the method does not terminate early, the Ritz pair (λ, \mathbf{u}) corresponding to an extremal eigenvector-eigenvalue pair (λ, \mathbf{v}) of T_j is an approximate eigenvalue-eigenvector pair of H . A rough measure of the quality of this approximation is given by the residual norm

$$\begin{aligned} \|H\mathbf{u} - \lambda\mathbf{u}\| &= \|HQ_j\mathbf{v} - Q_j T_j \mathbf{v}\| = \\ &= \beta_K |v_j|, \end{aligned}$$

which is given by the modulus of the last element in \mathbf{v} times β_K . The quality of the approximation usually increases with Krylov dimension K , with typical values of K ranging from a few dozens to a few hundreds.

The Lanczos method is famously ill-conditioned, resulting in loss of orthogonality, in finite precision arithmetic, of the constructed Krylov basis Q_j for modest sizes of K , and the appearance of spurious degeneracies (“ghost modes”) in the spectrum of T_j . We note that for the case of only computing a single extremal eigenvector, ghost modes are of no particular concern.

Algorithm 1 requires the storage of the constructed Krylov basis Q_j in memory. For large values of j this can become prohibitive. One can work around this issue by splitting Algorithm 1 into two separate runs. During

the first run one only computes the tridiagonal matrix T_j *without* storing the Krylov vectors Q_j . This requires only enough memory to store three consecutive Krylov vectors \mathbf{x}_n in memory. One then diagonalizes T_j to obtain the extremal eigenpair (λ, \mathbf{v}) . Finally, one uses the expansion coefficients \mathbf{v} as input to a second Lanczos run during which the desired extremal Ritz vector \mathbf{u} is accumulatively computed from the reconstructed Krylov

basis. The second run requires enough memory to store four Krylov vectors. The two algorithms are outlined in Algorithms 2 and 3. This approach of course comes at the expense of additional computational time required for the second run. This latter, memory-efficient implementation of Lanczos is what we use to find the ground state of a 1D spin chain and obtain for instance the results in Fig. 2.